

Disruption of mitochondrial electron transport chain function potentiates the pro-apoptotic effects of MAPK inhibition.

Andrew P. Trotta^{1,2}, Jesse D. Gelles^{1,3}, Madhavika N. Serasinghe^{1,2}, Patrick Loi¹, Jack L. Arbiser^{6,7}, and Jerry E. Chipuk^{1,2,3,4,5}

¹Department of Oncological Sciences,

²The Tisch Cancer Institute,

³The Graduate School of Biomedical Sciences,

⁴Department of Dermatology,

⁵The Diabetes, Obesity, and Metabolism Institute.

Icahn School of Medicine at Mount Sinai, One Gustave L. Levy Place, New York, NY 10029, USA

⁶Atlanta Veterans Administration Medical Center, Winship Cancer Institute

⁷Emory University, School of Medicine, Department of Dermatology, 1639 Pierce Dr, Atlanta, GA 30322, USA

Running title: Inhibition of mitochondrial respiration in cancer

To whom correspondence should be addressed: Dr. Jerry E. Chipuk. Department of Oncological Sciences, Icahn School of Medicine at Mount Sinai. One Gustave L. Levy Place, Box 1130, New York, New York 10029 USA. Telephone: +1 (212) 659-5543, Facsimile: +1 (212) 987-2240, Email jerry.chipuk@mssm.edu

Keywords: Mitochondria, respiration, electron transport chain, oncogenes, mitochondrial dynamics, apoptosis, targeted therapy.

ABSTRACT

The mitochondrial network is a major site of ATP production through the coupled integration of the electron transport chain (ETC) with oxidative phosphorylation. In melanoma, arising from the Val600Glu mutation in the kinase v-RAF murine sarcoma viral oncogene homolog B (BRAF^{V600E}), oncogenic signaling enhances glucose-dependent metabolism, while reducing mitochondrial ATP production. Likewise, when BRAF^{V600E} is pharmacologically inhibited by targeted therapies (*e.g.* PLX-4032/Vemurafenib), glucose metabolism is reduced and cells increase mitochondrial ATP production to sustain survival. Therefore, collateral inhibition of oncogenic signaling and mitochondrial respiration may help enhance the therapeutic benefit of targeted therapies. Honokiol (HKL) is a well-tolerated small molecule that disrupts mitochondrial function; however its underlying mechanisms and

potential utility with targeted anticancer therapies remain unknown. Using wild-type BRAF and BRAF^{V600E} melanoma model systems, we demonstrate here that HKL administration rapidly reduces mitochondrial respiration by broadly inhibiting ETC complexes I, II, and V, resulting in decreased ATP levels. The subsequent energetic crisis induced two cellular responses involving cyclin-dependent kinases (CDKs). First, loss of CDK1-mediated phosphorylation of the mitochondrial division GTPase dynamin-related protein 1 promoted mitochondrial fusion, thus coupling mitochondrial energetic status and morphology. Second, HKL decreased CDK2 activity, leading to G1 cell cycle arrest. Importantly, while pharmacological inhibition of oncogenic MAPK signaling increased ETC activity, co-treatment with HKL ablated this response and vastly enhanced the rate of apoptosis. Collectively, these findings integrate HKL action with mitochondrial respiration and shape and substantiate a pro-survival role of mitochondrial

function in melanoma cells following oncogenic MAPK inhibition.

Oncogenic MAPK mutations (i.e., a valine to glutamate amino acid substitution at residue 600 in v-RAF murine sarcoma viral oncogene homolog B, BRAF^{V600E}) occur within numerous tumor types, including malignant melanoma, colorectal, and ovarian cancers (1). The presence of the BRAF^{V600E} mutation results in hyperactivation of the MAPK pathway, leading to continuous cell cycle progression and proliferation. Consequently, inhibition of oncogenic MAPK signaling is a rational therapeutic strategy that can capture the majority of MAPK-driven cancers. For example, several small molecule inhibitors that target either BRAF^{V600E} (i.e., PLX-4032/Vemurafenib) or downstream effector proteins, such as MEK (i.e., GSK-1120212/Trametinib) have been approved for use in melanoma (2-6). Nevertheless, despite promising initial responses, melanoma patients invariably relapse from MAPK signaling inhibition within a year of treatment commencement (7,8). Several studies have now demonstrated reactivation of MAPK signaling as one of the primary causes for the development of treatment resistance (9-11). Therefore, the development of alternative strategies to eradicate cancer cells prior to treatment resistance is urgently required.

Oncogenic reprogramming of cellular metabolism is a hallmark of many cancers, whereby altered utilization of glucose and glutamine supports rapid proliferation. Indeed, a key feature of BRAF^{V600E} melanoma cells is the metabolic switch from mitochondrial respiration to glycolysis, which is termed the Warburg effect (12). Several mechanisms have been discovered to describe the Warburg effect in BRAF^{V600E} cancers, including increased glucose uptake and expression of glycolytic enzymes (12). However, recent work has demonstrated that changes in mitochondrial dynamics (i.e., mitochondrial fusion and fragmentation) play a critical role in regulating mitochondrial metabolism in both normal and cancer cells. For example, loss of function of the mitochondrial GTPase dynamin-related protein 1 (DRP1) causes fusion of the mitochondrial network and increases respiration (13,14). Conversely, oncogenic MAPK signaling increases

the expression and activity of DRP1, resulting in mitochondrial fragmentation and decreased respiration (13,15). Inhibition of BRAF^{V600E} in melanoma cells results in mitochondrial fusion, upregulation of oxidative phosphorylation genes, and increases mitochondrial biogenesis and respiration (13,16). These studies indicate that mitochondrial dynamics, oncogenic MAPK signaling, and cancer metabolism are intricately linked to tumorigenesis (17,18). Moreover, it is becoming evident that melanoma cells are dependent on mitochondria following inhibition of oncogenic MAPK signaling, and therefore may be vulnerable to compounds that disrupt mitochondrial function.

Honokiol (HKL) is a small molecule compound that has anti-cancer properties (19,20). Previous reports have demonstrated pro-apoptotic and anti-migratory effects of HKL in cancer cell lines and xenograft models of various malignancies, including breast (21), leukemia (22), and melanoma (23). Interestingly, recent work has shown that HKL can regulate mitochondrial function in normal and transformed cells (24,25). However, the underlying molecular action of HKL on mitochondrial function and morphology has not yet been characterized. In the current study, we demonstrate that HKL rapidly disrupts mitochondrial respiration by affecting complexes I, II, and V of the mitochondrial electron transport chain (ETC). The resulting energetic crisis causes distinct cellular phenotypes, including decreases in CDK1-mediated phosphorylation of DRP1, resulting in mitochondrial fusion, while decreases in CDK2 activity are associated with G1-cell cycle arrest. Furthermore, HKL can act as a single agent and in combination strategies with inhibition of oncogenic MAPK signaling to promote the mitochondrial pathway of apoptosis.

RESULTS

HKL induces mitochondrial dysfunction in melanoma cells by disrupting respiration - Currently, there is little mechanistic information regarding the action of HKL in mitochondria. However, two independent studies have indicated that HKL is able to rapidly enter mitochondria following administration to cells (24,25). We therefore began this study by first establishing if HKL has an immediate effect on mitochondrial respiration in melanoma cells. We utilized a

Seahorse Bioanalyzer to measure the basal oxygen consumption rates (OCR), a surrogate readout of mitochondrial respiration in A375 (BRAF^{V600E}), SKMEL-28 (BRAF^{V600E}), and MeWo (wild type BRAF) human malignant melanoma cell lines. Increasing doses of HKL resulted in a dose-dependent decrease in OCR in all cell lines tested (Figure 1A). At the highest concentration of HKL (40 μ M), OCR levels were reduced by 70%, 60%, and 46% in A375, SKMEL-28, and MeWo cells, respectively. Impressively, HKL-mediated decrease in mitochondrial respiration occurred within 5 minutes of drug administration to cells, indicating rapid cellular uptake and targeting of mitochondrial function. To further elucidate the time-dependent effects HKL has on mitochondrial function we assessed changes to OCR in cells treated with 40 μ M HKL for 8 hours. We found that HKL treated cells exhibited significantly reduced basal OCR (between 38-45%) compared to control treated cells (Figure 1B). Sequential administration of ETC complex inhibitors during these experiments allows for real-time assessment of different parameters associated with mitochondrial respiration. For example, oligomycin (complex V inhibitor) determines the amount of ATP production is linked to respiration, FCCP (mitochondrial uncoupler) enables measurement of maximal respiratory capacity, while a combination of rotenone (complex I inhibitor) and antimycin A (complex III inhibitor) determines the reserved respiratory capacity. We observed that HKL impaired all of these parameters compared to controls, indicating that HKL may inhibit multiple components of the ETC to repress overall cellular respiration (Figure 1B).

To further interrogate HKL-mediated mitochondrial dysfunction, we used TMRE and MitoSox dyes to evaluate mitochondrial membrane potential and mitochondrial reactive oxygen species (ROS) levels following treatment with HKL. Flow cytometry analysis revealed HKL dose-dependently decreases in mitochondrial membrane potential with the highest concentration of HKL (40 μ M) reducing membrane potential between 15-22% after 8 hours (Figure 1C). Conversely, HKL treatment resulted in a dose-dependent increase in ROS production (140-160% increase at 40 μ M HKL) in all cell lines tested (Figure 1D). As expected, treatment with the mitochondrial uncoupler FCCP resulted in the

maximal loss of membrane potential (70-89% decrease) and increase in ROS production (400-500%) in all cell lines (Figure 1D). Importantly, the doses and timing of HKL treatment used in these experiments did not induce apoptosis (i.e., Annexin V positivity) or cell cycle arrest (Supplementary Figure 1A-1B), indicating that HKL-mediated decreases in mitochondrial function are direct and are not due to secondary effects on the cell cycle or induction of cell death pathways.

Mitochondrial dysfunction caused by HKL occurs through loss of Complex I, II, and V activity - Given the potent inhibitory effect HKL has on mitochondrial respiration, we hypothesized that HKL acts to inhibit 1 or more ETC complexes. To investigate this, we utilized the Seahorse Bioanalyzer and used OCR as a surrogate readout of individual ETC complex activity following the addition of ETC metabolites and complex inhibitors (26). A375 cells were treated with either DMSO or 40 μ M HKL for 8 hours followed by permeabilization of the plasma membrane with recombinant perfringolysin O to ensure sufficient delivery of metabolites to mitochondria. Complex I activity was assessed by the addition of pyruvate, malate, and ADP. Pyruvate activates dehydrogenase subunits within complex I, while malate prevents the accumulation of acetyl CoA, which at high concentrations can inhibit pyruvate dehydrogenase activity (26). The inclusion of ADP maintains the mitochondria in a state of energy stimulated oxygen consumption. In control treated cells, the addition of complex I substrates increases OCR, while the subsequent addition of rotenone inhibits complex I activity, and consequently reduces OCR (Figure 2A). This reduction was reversed following the administration of the complex II metabolite succinate. Finally, to determine the maximal respiratory capacity of these cells we administered FCCP, and found no additional increase in OCR, indicating that the concentration of succinate (10mM) used in these experiments was sufficient to cause maximal respiration (Figure 2A). Likewise, we observed that HKL treated A375 cells followed the same pattern of OCR responses after the addition of each compound (Figure 2A). Importantly however, the magnitude of responses was significantly lower compared to control treated cells, indicating that complex I activity was

impaired, and that the addition of succinate was not sufficient to rescue respiration (Figure 2A). These findings were confirmed in SKMEL-28 cells (Supplementary Figure 2A).

To expand upon these findings we assessed the effect of HKL on complex I activity using an enzymatic ELISA-based assay. A375 cells were treated with either DMSO or 40 μ M HKL for 24 hours. We purified the mitochondrial fractions as previously described (27), immunoprecipitated complex I, and measured the rate of oxidation of NADH to NAD⁺ (i.e., complex I activity). There was a 37.2% reduction in the rate of complex I activity in HKL treated cells compared to control, suggesting that indeed HKL targets complex I to reduce respiration (Figure 2B). Given this assay specifically measures NADH dehydrogenase activity; we hypothesized that HKL-mediated complex I impairment could be due to decreased expression of NADH dehydrogenase (ND) subunits. Quantitative real time PCR analysis revealed that *ND1* gene expression was reduced by 2.3 fold in HKL treated A375 cells compared to controls, while the expression of all other ND subunits (*ND2-6*) remain unchanged (Figure 2C). This decrease in *ND1* mRNA expression correlated with a similar decrease in ND1 protein levels (Figure 2D).

The above findings indicate that HKL mediates disruption of complex I activity through loss of expression of ND1. However, our earlier results indicate that either immediate administration (Figure 1A) or short-term treatment (i.e., 8 hours; Figures 1B, 2A) of HKL reduces respiration, suggesting that HKL may directly affect complex I activity. To answer this possibility we isolated heavy membrane fractions from mouse livers and treated them with either DMSO or 40 μ M HKL for 30 minutes at room temperature followed by measurement of complex I activity. The rate of complex I enzymatic activity was attenuated by 23% in HKL treated mitochondria compared to controls (Figure 2E). The ETC complexes are located within the inner mitochondrial membrane and are organized in a solid state system where individual complexes can assemble to form supercomplexes, which increases the efficiency of electron transfer and respiration (28,29). We therefore asked if the context of complex I within the inner mitochondrial membrane, proximity to other ETC complexes,

and other mitochondrial co-factors is essential for HKL-mediated inhibition of complex I activity. Mouse liver mitochondria were lysed, and complex I was separated from other mitochondrial components by immunoprecipitation either in the presence or absence of HKL. Following 3 hours incubation, HKL was able to inhibit isolated complex I activity by 17.5% compared to control, indicating that HKL directly targets complex I activity (Figure 2F).

Although complex I is a possible target for HKL, the decrease in complex I activity appears to be relatively minor when compared to overall loss in mitochondrial respiration as assessed by our earlier Seahorse analysis (Figure 1A-1B), which indicates other ETC complexes may be involved. Mitochondrial respiration can be maintained via the donation of electrons from FADH₂ to complex II. Indeed, our initial cell permeabilization experiments demonstrated ineffective succinate-mediated recovery of OCR in HKL treated cells (Figure 2A), indicating that HKL may be acting downstream of complex I. To assess if complex II is also being affected by HKL, we permeabilized DMSO or HKL pre-treated A375 and SKMEL-28 cells and administered a combination of rotenone, succinate, and ADP to specifically assess complex II activity independently of complex I. The addition of succinate increased OCR by 3.5 fold in control treated cells compared to a 2.3 fold increase in HKL treated cells (Figure 2G, Supplementary Figure 2B), suggesting that HKL impairs complex II activity. The addition of oligomycin, FCCP, and antimycin A further demonstrates that all other respiration parameters are impaired in HKL treated cells, which is most likely a consequence of HKL acting on multiple components of the ETC (Figure 2G). To confirm complex II is directly inhibited by HKL, we conducted complex II ELISA-based enzymatic activity assays using mouse liver mitochondria treated with either DMSO or HKL for 30 minutes at room temperature. These experiments revealed that HKL reduces the rate of complex II enzymatic activity by 21.9% compared to control (Figure 2H). Finally, we examined the effect inhibition of complex I and II has on ATP production, which is a measure of complex V activity. To answer this we treated melanoma cells with or without HKL for 8 hours and measured OCR following the addition of oligomycin and found that HKL

decreases ATP production between 44-66% in all cell lines tested (Figure 2I). Collectively, these data show that HKL specifically affects the activity of ETC complexes I, II, and V to reduce mitochondrial respiration.

HKL-mediated energetic crisis results in mitochondrial fusion via loss of CDK1-mediated DRP1 phosphorylation at serine 616 - Thus far, we have shown that HKL acts as an inhibitor of mitochondrial respiration, but an effect of HKL on mitochondrial function still remains unknown. Mitochondria are dynamic organelles capable of altering their shape, size, and sub-cellular localization to meet specific energetic and biological requirements (17). As such, a structural-functional relationship exists between specific mitochondrial shapes and their energetic states. For example, activation of the mitochondrial division protein DRP1 is essential for mitochondrial fragmentation during mitosis to ensure equal distribution of mitochondria to daughter cells (30). Fusion of the outer mitochondrial membrane is mediated by mitofusin 1 and 2 (MFN1 and MFN2), while inner mitochondrial membrane fusion is regulated by OPA1. Given our findings show that HKL induces an energetic crisis via ETC inhibition, we hypothesized subsequent changes in mitochondrial shape as a means of energetic compensation. A previous study demonstrated that oncogenic BRAF^{V600E} signaling promotes a fragmented mitochondrial network through ERK-mediated phosphorylation of DRP1 at serine 616 (DRP1 Ser616), a marker of active DRP1 (13). The specific BRAF^{V600E} inhibitor PLX-4032 (PLX) effectively silences this pathway and results in mitochondrial fusion (13). We assessed mitochondrial morphology within A375, SKMEL-28, and MeWo cells using live cell fluorescent microscopy following treatment with DMSO and HKL, while PLX was used as a control drug that induces changes in mitochondrial morphology. Control treated A375 and SKMEL-28 cells contain a fragmented mitochondrial phenotype, whereas the mitochondrial network in MeWo cells was more fused and interconnected (Figure 3A). Treatment with HKL resulted in mitochondrial fusion in A375 and SKMEL-28 cells, but did not affect MeWo cells (Figure 3A-3B). As expected, PLX induced mitochondrial fusion in the BRAF^{V600E} positive A375 and SKMEL-28 cells.

As MeWo cells are wild type for BRAF there was no effect of PLX on mitochondrial shape in these cells (Figure 3A-3B, Supplementary Figure 3A).

To investigate the mechanism through which HKL treatment induces fusion of the mitochondrial network, we screened for changes within the mitochondrial dynamics machinery at both the mRNA transcript and protein levels. HKL treatment did not significantly alter the expression of the mitochondrial machinery, nor were there any changes in total DRP1, MFN1, MFN2, and OPA1 protein levels (Figure 3C-3D). However, DRP1 Ser616 levels were significantly lower in HKL treated cells (Figure 3D). As expected, inhibition of BRAF^{V600E} with PLX resulted in a decrease in DRP1 Ser616 levels (Figure 3D). We further integrated these results by determining how HKL affects the colocalization of DRP1 Ser616 with fused or fragmented mitochondria. Using immunofluorescence, SKMEL-28 cells were stained for DRP1 Ser616 and HSP60, a mitochondrial matrix marker. Under control conditions, DRP1 Ser616 protein colocalized with fragmented mitochondria (Supplementary Figure 3B). Cells treated with HKL displayed reduced DRP1 Ser616 associated with mitochondria, while PLX completely eliminates the colocalization between DRP1 Ser616 and fused mitochondria (Supplementary Figure 3B). Collectively, these data indicate that HKL-mediated mitochondrial fusion occurs through inhibition of DRP1 and decreased mitochondrial fragmentation in BRAF^{V600E} melanoma cells. A previous study demonstrated that oncogenic MAPK signaling promotes both increased glucose uptake and DRP1 activity (13). Given this relationship between oncogenic signaling, cellular metabolism, and mitochondrial shape, we were interested in assessing the effect glucose depletion and DRP1 knockdown has on mitochondrial respiration. SKMEL-28 cells were infected with pSUPER or shDRP1 and cultured for 72 hours. Depletion of glucose results in a moderate increase in both basal and maximal OCR (Figure 3E; black bars), an effect that was exacerbated after knockdown of DRP1 (Figure 3E-3F), suggesting that DRP1 plays an important role in regulating mitochondrial respiration. Given that HKL inhibits both mitochondrial respiration and DRP1 phosphorylation, we wanted to assess if this was a common phenotype exhibited by other ETC

inhibitors. Indeed, western blot analysis demonstrated that inhibition of complex I (rotenone), complex III (antimycin A), or complex V (oligomycin) all reduce DRP1 Ser616 levels, albeit to a lesser degree than HKL or PLX (Figure 3G). We did not observe any decrease in DRP1 Ser616 levels with metformin, a complex I inhibitor, which may be due to the fact that it has a lower potency in inhibiting complex I compared to rotenone (31).

HKL is a potent inhibitor of various oncogenic signaling pathways, including PI3K/mTORC and MAPK signaling in glioblastoma cells (32,33). Given that HKL and PLX both act to decrease DRP1 Ser616 levels, we asked if the mechanism of HKL-mediated inhibition of DRP1 was through blocking MAPK signaling. Using ERK phosphorylation (pERK) as a readout of active MAPK signaling, we demonstrated that treatment with PLX for 24 hours significantly decreases pERK levels in A375 and SKMEL-28 cells, respectively (Figure 3H). However, we did not observe any decrease in pERK or total ERK with increasing HKL concentrations, suggesting HKL does not inhibit oncogenic MAPK signaling in these melanoma cells. Nonetheless, HKL did reduce DRP1 Ser616 levels, indicating that HKL may act on DRP1 through alternative mechanisms (Figure 3H). It has been previously documented that during mitosis, DRP1 is phosphorylated at Ser616 by cyclin-dependent kinase 1 (CDK1) (34,35). We therefore assessed if HKL affect CDK1 activity via phosphorylation of threonine 161 (CDK1 T161), which is representative of active CDK1. Western blot analysis showed that HKL reduces CDK1 T161 levels in all melanoma cell lines (Figure 3I). Total CDK1 was slightly lower in HKL-treated A375 cells, but remained unaffected in SKMEL-28 and MeWo cells (Figure 3I). Finally, to further integrate the inhibitory effect of HKL on CDK1 activity, we examined the phosphorylation status of protein phosphatase 1 (PP1), a known CDK1 substrate (36). Western blot analysis revealed that HKL treated melanoma cells have decreased phosphorylation at threonine residue 320 (PP1 T320; Figure 3I), indicating that HKL targets CDK1 and affects its downstream substrates. Collectively, these data suggest that HKL-induction of mitochondrial fusion occurs

through loss of CDK1-mediated activation of DRP1.

HKL promotes CDK2-mediated cell cycle arrest and induces the mitochondrial pathway of apoptosis - The finding that CDK1 activity is targeted by HKL prompted us to hypothesize that HKL treatment would result in G2-M arrest of the cell cycle, as this phase of the cell cycle is regulated by CDK1. Surprisingly, cell cycle analysis demonstrated that HKL treated cells arrested in the G1 phase of the cell cycle (Figure 4A). As a control, PLX treatment induced G1-cell cycle arrest in A375 and SKMEL-28, but not MeWo cells as expected. These data suggests that HKL might target a regulator of G1-S transition. To elucidate the underlying mechanism for the G1-arrest phenotype, we examined the phosphorylation status of CDK2, a known regulator of the G1/S transition. HKL treatment decreased phosphorylation of CDK2 at the threonine residue 160 (CDK2 T160), which is indicative of active CDK2, while total CDK2 levels were unaffected (Figure 4B). Collectively, these findings suggest that loss of CDK2 activity mediates G1-cell cycle arrest, while the decrease in CDK1 prevents the phosphorylation of DRP1.

Previously published literature on the effects of HKL in cancer cells confirms a cell cycle arrest phenotype, but also indicates that HKL is a potent inducer of cell death (19,20). Although the mechanism of HKL-induced cell death remains unclear, several studies have indicated that HKL can downregulate the anti-apoptotic proteins BCL-2 and BCL-xL (37,38). However, western blot analysis of A375 cells treated with DMSO or HKL found no change in BCL-xL protein levels, or changes in protein levels other pro- and anti-apoptotic BCL-2 proteins (Figure 4C). To characterize the cell death response, we performed kinetic apoptosis assays as measured by Annexin V staining, which demonstrate that 40 μ M HKL is capable of inducing cell death over the course of 40 hours (Figure 4D). To determine if this cell death phenotype is apoptosis we pre-treated cells with zVAD-fmk, a pan-caspase inhibitor, or co-treated with HKL and ABT-737, a small-molecule inhibitor to several anti-apoptotic BCL-2 proteins (i.e., BCL-2, BCL-xL, and BCL-W). These compounds are well tolerated by cells as single agents (Figure 4E). Pre-treatment with zVAD-fmk

reduced HKL-mediated cell death, while combination of HKL with ABT-737 increases Annexin V staining, indicating that the mechanism of cell death is the mitochondrial pathway of apoptosis (Figure 4F). Given the effects of HKL on mitochondrial shape, we asked if the presence of DRP1 was important for HKL-mediated apoptosis to proceed. Knockdown of DRP1 in SKMEL-28 did not significantly alter the induction of HKL-mediated apoptosis (Figure 4G), indicating that DRP1 does not play any significant role in mediating HKL-induced apoptosis. Finally, colony formation assays indicate that increasing doses of HKL causes a marked reduction in long-term clonogenic survival of melanoma cell lines (Figure 4H). Collectively, these data indicate that HKL is an inhibitor of the cell cycle by reducing the activity of CDK2, while also inducing the mitochondrial pathway of apoptosis.

MAPK inhibition increases respiration and sensitizes melanoma cells to HKL-induced apoptosis - Oncogenic MAPK signaling promotes glycolysis and inhibits mitochondrial respiration (12,13). While MAPK pathway inhibitors are not potent cell death inducers as single agent, they effectively block MAPK signaling and induce cell cycle arrest (Figure 3G, 4A). We hypothesize that an additional consequence of MAPK inhibition is increased respiration, which will sensitize cells to ETC inhibitors, such as HKL. Indeed, treatment with PLX or the MEK inhibitor GSK-1120212 (GSK) increases cellular respiration, while HKL decreases OCR levels consistent with our earlier data (Figure 5A). We also increased the concentration of PLX (10 μ M) and GSK (50nM) and assessed apoptotic responses over time. Both drugs were able to induce a moderate apoptotic response after 30 hours of treatment (Figure 5B). Importantly, the combination of PLX with either 20 or 40 μ M HKL significantly enhances the rate of apoptosis, while a similar response was observed with the combination of GSK and HKL (Figure 5C-5D). Finally, the combination of these drugs at lower doses significantly decreased clonogenic survival (Figure 5E, Supplementary Figure 4). These data demonstrate that inhibition of MAPK signaling markedly increases mitochondrial respiration, which sensitizes melanoma cells to HKL-induced apoptosis.

DISCUSSION

This study reveals several underlying mechanisms of how HKL disrupts mitochondrial function in melanoma cancer cells (Figure 5F). In brief, we demonstrate that HKL is a potent inhibitor of mitochondrial respiration by decreasing the activities of ETC complexes I, II, and V (Figures 1A-1B, 2A-2B, 2E-2H, 2I); HKL induces fusion of the mitochondrial network by inhibiting the CDK1-DRP1 axis (Figure 3A, 3I); and finally, HKL synergizes with MAPK inhibitors to enhance apoptotic responses (Figure 5A-5F). Collectively, these data represent novel HKL modalities that impinge on mitochondrial function, and highlight the impact of small molecules that target mitochondrial ATP production as anti-cancer strategies.

Oncogenic signaling, such as BRAF^{V600E} in melanoma, actively adjusts cellular metabolism towards glycolysis in order to support the high energetic and anabolic demands of rapidly proliferating cancer cells (12). Furthermore, glucose dependency within these cancers is the foundation by which clinical imaging techniques (i.e., positron emission tomography) map metabolic responses before and after treatment. Indeed, clinical results demonstrate a complete loss of glucose uptake by BRAF^{V600E} positive melanomas following treatment with PLX-4032, however there is considerable variation in responses with reduction in tumor burden, suggesting that alternative pathways are active to maintain ATP production and cancer cell survival (39,40). In the current study, we demonstrate that PLX-4032 and GSK-1120212 increase mitochondrial respiration in BRAF^{V600E} melanoma cells (Figure 5A). Importantly, we show that the dependency on mitochondrial respiration following oncogenic MAPK inhibition sensitizes melanoma cells to HKL-induced apoptosis and decreases clonogenic survival (Figure 5B-5E).

Melanomas have complex genetic and mutational expression profiles (41), which consequently limit the clinical utility of MAPK inhibitors through intrinsic and acquired mechanisms of resistance. Intrinsic resistance refers to melanoma cells that, in addition to BRAF^{V600E}, contain additional genetic alterations, mutations, and/or amplifications (i.e., loss of *PTEN*, amplification of cyclin D1) that override anti-proliferative effect of MAPK inhibition (42). Conversely, acquired resistance to MAPK

inhibition frequently occurs within 6-8 months following treatment, and is usually due to reactivation of the MAPK pathway (7-11). As single agent therapies, inhibition of MAPK signaling induces apoptosis in only a small fraction of cells, while the remainder either enter cell cycle arrest to stabilize disease or do not demonstrate a clinically response (i.e., intrinsically resistant). The subpopulation of cancer cells that display intrinsic resistance to MAPK inhibitors tend to have high rates of mitochondrial biogenesis and are metabolically dependent on mitochondrial respiration (43). The information provided here suggests that this subpopulation of melanoma cells may be sensitive to HKL-induced mitochondrial dysfunction and apoptosis. Consequently, a window of opportunity for alternative therapeutic intervention before reactivation of MAPK signaling and subsequent treatment relapse is often lost. Combined targeting of mitochondrial respiration and oncogenic MAPK signaling, such as HKL and PLX-4032 as presented here may prevent the selection of resistant tumor cells and improve overall patient survival. It would be interesting to further evaluate HKL and MAPK inhibitors using *in vivo* models of melanoma to establish if simultaneous inhibition of oncogenic signaling and mitochondrial respiration promotes durable responses and ultimately cancer cell apoptosis.

A recent report suggested that HKL negatively affected mitochondrial respiration in non-small cell lung cancer; however the mechanism was not characterized (24). Our study reveals that HKL directly targets complexes I, II, and V of the ETC (Figure 2A-2B, 2E-2I), which causes a state of energetic crisis, and ultimately, induction of cell death (Figure 4D). We discovered that complex I activity was inhibited by both direct administration of HKL as well as loss of *ND1* expression following longer treatment (Figure 2C-2D). The observation that HKL is able to rapidly decrease complex I activity, indicates that may influence complex activity, stability, or assembly. The complex I enzymatic assay used in this study measures the rate of NADH dehydrogenase activity, which is not dependent on ubiquinone to shuttle electrons between complexes I-III. Inhibitors that bind at or near ubiquinone sites (i.e., rotenone) are ineffective at inhibiting complex I activity in this assay. In this context,

our data suggests that HKL does not decrease respiration by affecting the transfer of electrons between complexes, but most likely directly inhibits NADH dehydrogenase activity. Similarly, we found that HKL diminishes the activity of complex II and V, possibly indicating congruent modes of HKL action between ETC complexes. Alternatively, inhibition of multiple ETC complexes by HKL suggests that this drug may also influence mitochondrial ultrastructure or supercomplex assembly (44).

The underlying notion that inhibiting ETC function is an effective anti-cancer strategy is supported by use of metformin in cancer patients (45). Metformin, a type II diabetic drug and complex I inhibitor, has been associated with decreased risk of cancer development while also possessing anti-cancer properties *in vitro* and *in vivo* (45). However, metformin requires organic cation transporters (OCTs) that are only expressed in a few tissues, such as the liver and kidney (46). Likewise, not all cancer cells express OCTs, indicating a potentially low therapeutic index for metformin in certain cancer patients (46). Other ETC inhibitors, such as rotenone (complex I), antimycin A (complex III), and oligomycin (complex V), are either highly toxic or have poor pharmacokinetic properties. HKL is a non-toxic, small molecular weight biphenolic compound capable of inhibiting mitochondrial respiration without the requirement for specific transporters. Moreover, HKL is derived from the bark of *Magnolia grandiflora*, which has been used in traditional Chinese medicine for centuries without any appreciable toxicity (47,48), indicating that HKL displays two selective advantages over current ETC inhibitors. First, HKL simultaneously targets multiple ETC complexes, and second it is well tolerated by normal cells (48). While there are no known mitochondrial respiratory inhibitors that specifically act within neoplastic cells, it appears the activity of HKL in normal and cancer cells fits within a general class of phenolic compounds, including curcumin and resveratrol. In cancer cells, these compounds inhibit complex V activity, resulting in decreased ATP production, mitochondrial membrane potential, increased ROS generation and apoptosis (49). Whether or not other phenolic compounds share similar properties to HKL, such as inhibiting ETC complex I and II in cancer cells remains unknown. Conversely, in

normal cells phenolic compounds have cytoprotective effects. For example, both HKL and resveratrol prevent cardiac hypertrophy by enhancing mitochondrial respiration via a Sirt3-dependent mechanism (25,50), suggesting the phenolic class of small molecules have distinct effects in non-neoplastic and cancer cells. This may highlight a role for mitochondrial ultrastructure and shape mediating the tissue and cellular responses to HKL.

An additional finding from our study is that HKL causes mitochondrial fusion following a decrease in phosphorylated DRP1 Ser616 levels (Figure 3A, 3D). Interestingly, this loss of function did not occur through inhibition of oncogenic MAPK signaling, but rather through loss of CDK1 activity (Figure 3H-3I). Similarly, we found CDK2 is a HKL target resulting in G1 cell cycle arrest (Figure 4B). Previous studies found that HKL induces a similar cell cycle arrest phenotype, albeit through targeting the G1 regulators CDK4 and CDK6 (51-53), indicating that HKL may act as a pan-CDK inhibitor. The recent resurgence in developing targeted therapies against cell cycle regulators, such as CDKs, suggests this approach to be a viable anti-cancer strategy. However, given the level of redundancy across the CDK family (with the exception of CDK1), developing specific cell cycle inhibitors has thus far been problematic, while pan-CDK inhibitors are highly toxic (54). The ability of HKL to target multiple CDKs with a high therapeutic index, suggests that it may overcome many of the issues surrounding previous CDK inhibitors. Taken together, this study illuminates how HKL affects mitochondrial respiration, mainly through the inhibition of ETC activity, and provides insights into the therapeutic rationale of dual inhibition of oncogenic signaling and mitochondrial function in melanoma.

EXPERIMENTAL PROCEDURES

Cell lines and reagents - All cell culture and transfection reagents were obtained from ThermoFisher Scientific (MA, USA) and standard reagents were from Sigma-Aldrich (MO, USA) or Fisher Scientific (NH, USA). A375, SK-MEL-28 and MeWo lines were obtained from American Type Cell Culture (ATCC) and were maintained in Dulbecco's modified Eagle's medium (DMEM) containing 10% fetal bovine serum, 2mM L-glutamine, and 1% antibiotics. Drugs were

obtained from: ABT-737 (Abbott Laboratories; Abbott Park, IL, USA), PLX-4032/GSK-1120212 (Selleck Chemicals; TX, USA), zVAD-fmk (Calbiochem/Millipore; Darmstadt, Germany), Hoechst-33342 (Anaspec; CA, USA), CHX (Sigma-Aldrich; MO, USA). Honokiol was kindly provided by the laboratory of Jack Arbiser (Emory University School of Medicine, Atlanta, Georgia, USA). Antibodies are presented in Supplementary Table 1.

Seahorse analyses - For mitochondrial respiration experiments, cells were seeded in XFe96 plates (Agilent; CA, USA) using the following plating densities: A375 (100,000 cells/well), SKMEL-28 (80,000 cells/well), MeWo (100,000 cells/well), and treated with DMSO or 40μM HKL for 8 hrs. Oxygen consumption rates (OCR) were measured using the XFe96 Extracellular Flux Analyzer and the XF Cell Mito stress test kit (Agilent) according to the manufacturer's instructions. Briefly, media containing treatments were aspirated and cells were washed once with unbuffered XF Mito stress media (DMEM supplemented with 100mM glucose, 200mM glutamine and 100mM pyruvate, pH 7.4). Cells in XF Mito stress media were incubated at 37°C in the absence of CO₂ for 1 hr. Baseline OCR measurements were determined before administration of oligomycin (1μM), carbonyl cyanide-4-(trifluoromethoxy)phenylhydrazone (FCCP: 1μM), and a combination of rotenone and antimycin A (0.5μM). Cells were stained with methylene blue, de-stained, and the absorbance was measured at 668nm using a plate reader (Synergy H1 Hybrid multi-mode micro-plate reader, Biotek). OCR measurements were normalized against the cell densities and all data analysis was conducted with the Seahorse Wave software version 2.2.0.276 (Agilent). For cell permembrilization experiments, cells were seeded in XFe96 plates and treated with DMSO or 40μM HKL for 8 hrs. Media was removed and cells were washed in 1× Mitochondrial Assay Buffer (MAS: 220mM Mannitol, 70mM Sucrose, 10mM KH₂PO₄, 5mM MgCl₂, 2mM HEPES, 1mM EGTA, 0.2% fatty acid free BSA). Cells in 1× MAS buffer containing 1nM plasma membrane permeabilizer (Agilent) were incubated at 37°C in the absence of CO₂ for 30 mins. Baseline OCR measurements were recorded before administration of complex

metabolites and/or inhibitors as indicated. OCR measurements were normalized to total cell number as indicated above.

Mitochondrial membrane potential ($\Delta\phi_M$), mitochondrial reactive oxygen species (mtROS) measurements - Cells seeded (60,000 cells/well) in 48 well plates were treated with either DMSO or increasing doses of HKL for 8 hrs or with 50 μ M FCCP for 2 hrs at 37°C. Either 100nM tetramethylrhodamine ethyl ester [TMRE] (ThermoFisher Scientific) or 5 μ M MitoSOX (ThermoFisher Scientific) was added, incubated at 37°C for 30 mins, trypsinized, and analyzed on a Canto II flow cytometer (BD Biosciences; CA, USA).

Cell cycle assays - Cells were seeded (100,000 cells/well) in 12 well plates and treated as indicated for 24 hrs. Cells were harvested by trypsinization, fixed in ice-cold 70% ethanol with gentle vortexing, and incubated at 4°C overnight. The following day, the cells were pelleted, washed twice with ice-cold 1 \times PBS, and resuspended in 1 \times PBS containing 60 μ g/ml propidium iodine and 50 μ g/ml RNase (Qiagen; MD, USA), and incubated at room temperature for 30 mins. Cells were analyzed on a Canto II flow cytometer (BD Biosciences).

Heavy membrane isolations - Cells were seeded in 15 cm dishes and treated with either DMSO or 40 μ M HKL for 24 hrs. Cells were harvested by trypsinization and centrifuged at 1000 \times g for 10 mins. Heavy membrane fractions (i.e., mitochondria) were isolated as previously described (27). Briefly, cell pellets were washed once in 1 \times PBS and resuspended in mitochondrial isolation buffer (MIB: 200mM mannitol, 68mM sucrose, 10mM HEPES-KOH pH 7.4, 10mM KCL, 1mM EDTA, 1mM EGTA, 0.1% BSA) supplemented with protease inhibitors (ThermoFisher Scientific). Cells were incubated on ice for 20 mins, and homogenized using a 2ml Potter-Elvehjem dounce. To ensure proper clearance of unlysed cells and nuclei, the homogenate was subjected to two rounds of centrifugation at 800 \times g for 10 mins at 4°C. The resulting supernatant was centrifuged for 10 mins at 8000 \times g at 4°C, supernatants were aspirated and the pellet was collected as the heavy membrane fraction. Pellets were resuspended in 100 μ L MIB and quantified by absorbance at 520nm. An

absorbance reading of 0.25 equates to ~20mg/mL. Samples were diluted to 100 μ g and subjected to SDS-PAGE and western blot analyses.

Complex I and II enzymatic ELISA - Complex I and II enzymatic activity measurements was performed using enzyme microplate kits (Abcam; MA, USA) and heavy membrane isolates from wild type BALB/C mouse livers and A375 and SKMEL-28 cells. Briefly, A375 and SKMEL-28 cells were treated with either DMSO or 40 μ M HKL for 24 hrs. Heavy membranes were isolated as described above. Mouse liver mitochondrial isolations were performed as described (27). Total protein concentrations were quantified using the Pierce BCA protein assay kit (ThermoFisher Scientific) and between 10-100 μ g of mitochondrial proteins were used in each assay. Complex I and II activity assays were performed according to manufacturer's instructions and kinetic measurements were recorded by absorbance readings at 450nm and 600nm, respectively every 30 secs for 60 mins.

Live cell imaging - Cells were seeded (40,000 cells/6cm plate) for 24 hrs before indicated treatments. Mitochondria and nuclei were labelled with 100nM Mito Tracker Green (ThermoFisher Scientific) and 4 μ M Hoechst 33342 (ThermoFisher Scientific) for 30 mins at 37°C, respectively. All imaging was performed on a Zeiss Imager.Z1 equipped with an N-Achroplan 40 \times /0.75 water immersion lens and an AxioCAM MRm digital camera. Images were captured using AxioVision 4.8 and Zeiss Zen software (Zeiss; NY, USA).

Immunofluorescence - SKMEL-28 cells were seeded (10,000/chamber) 1.8cm² Nunc™ Lab-Tek™ chamber slides (ThermoFisher Scientific) for 24 hrs before indicated treatments. Cells were washed with 1 \times PBS, fixed in 4% formaldehyde, and incubated in blocking buffer (1 \times PBS supplemented with 5% normal goat serum and 0.3% Triton™ X-100) for 60 mins at room temperature. Primary antibodies for DRP1 Ser616 (1:3200) and HSP60 (1:300) were diluted in 1 \times PBS supplemented with 1% BSA and 0.3% Triton™ X-100, and incubated overnight at 4°C. Cells were washed 3 times/5 mins with PBS and the secondary antibodies Alexa Fluor® 488 (1:1000, Cell Signaling) and Texas Red (1:200, Cell Signaling) were diluted in the above primary

antibody buffer and incubated for 90 mins at room temperature in the dark. Cells were washed 3 times/ 5mins in PBS, and then mounted with ProLong® Gold Antifade Reagent containing DAPI, cured overnight at room temperature, and imaged with a Zeiss Imager.Z1 at 40× magnification and an AxioCAM MRm digital camera, images were captured using AxioVision 4.8 software.

SDS-PAGE analyses - To generate whole cell protein lysates, cells were treated as indicated, trypsinized, pelleted, and washed in 1× PBS. Cell pellets were resuspended in RIPA buffer (1× PBS containing 1% Nonidet P-40, 0.5% sodium deoxycholate, 0.1% sodium dodecyl sulfate) supplemented with protease inhibitors (HALT; Pierce Biotechnology). Cells were incubated on ice for 20 mins and centrifuged for 10 mins at 21,000×g at 4°C. Quantification of lysates was performed using the Pierce BCA protein assay kit (ThermoFisher Scientific). Proteins (30-50µg/lane) were subjected to SDS-PAGE before transferring to nitrocellulose by standard western blot protocols and blocked in 5% milk/TBST. Primary antibodies (1:1000 in blocking buffer) were added to membranes and incubated overnight at 4°C. Blots were washed 3 times/10 mins with TBST and the secondary antibody (1:2000 in blocking buffer) was incubated at room temperature for 30 mins followed by 3 times/10 mins TBST wash steps. Protein bands were detected by standard enhanced chemiluminescence detection and exposure to film.

Quantitative real time PCR - Total cellular RNA extractions and first strand cDNA synthesis were performed as described (13). Gene expression was analyzed using SYBR Green detection [FastStart Universal SYBR Green Master Mix, (Roche)] and Applied Biosciences ViiA 7 Real-Time PCR system (ThermoFisher Scientific). Relative gene expression was determined using the comparative C_T method and normalized to 18S. Primer sequences for all genes investigated are located in Supplementary Table 2.

RNA interference and stable clone generation - The human pSUPER-shDRP1 plasmid was kindly provided by Dr. David Kashatus (University of Virginia, School of Medicine, Charlottesville, Virginia, USA) and scrambled shRNA construct was kindly provided by the laboratory of Dr. R. Premkumar Reddy (Icahn School of Medicine at Mount Sinai). HEK-293T cells were used to produce lentiviral particles for the generation of stable scramble shRNA and shDRP1 cell lines. Virus supernatants were harvested at 48 and 72 hrs, pooled, and 0.45µm filtered. SKMEL-28 stable clones were generated using puromycin (0.5mg/ml).

Apoptosis and clonogenic survival assays - For Annexin V cell death assays, cells were seeded for 24 hrs and treated as indicated. Floating and attached cells were harvested, stained with AnnexinV-FITC in binding buffer (10mM HEPES pH 7.4, 150mM NaCl, 5mM KCl, 1mM MgCl₂, 1.8mM CaCl₂), and analyzed by flow cytometry as described (13). For IncuCyte ZOOM (Essen Bioscience; MI, USA) experiments, cells were plated in 96 well plates and treated where indicated with Annexin V labelled with AlexaFluor 594 NHS ester (ThermoFisher Scientific) as described (55). Briefly, experiments were conducted for 24-48 hrs with data collection every 2 hrs using a 10× objective lens. Data was processed and analysed using the IncuCyte ZOOM software package (Version 6.2.9200.0). Processing definitions are presented in Supplementary Table 3. Clonogenic survival studies were performed by seeding cells in 24 well plates and treated every two days as described until control treated cells reach confluency. Colonies were stained with methylene blue and imaged. De-staining buffer (20% methanol in 5% acetic acid) was added to each well and measured for absorbance at 668nm using a microplate reader (Biotek).

Statistical analyses - Statistical analyses were performed as indicated in the figure legends. Student T tests were performed in Microsoft Excel to determine statistical differences between two groups. Significance was set at $p < 0.05$.

Acknowledgements

We would like to thank everyone in the J.E.C. laboratory for assistance and support. We would also like to thank Dr. Robert Fisher and members of his laboratory (Icahn School of Medicine at Mount Sinai) for critical reagents and assistance.

Conflict of Interest

The authors declare no conflict of interest.

Author contributions: A.P.T. and J.E.C. were involved in the conception and design of experiments. A.P.T., P.L., J.D.G., M.N.S. and J.E.C. were involved in data acquisition, analysis, and interpretation. A.P.T. and J.E.C. prepared figures and wrote the manuscript. All authors were involved in critically reviewed the results and approved the final version of the manuscript.

REFERENCES

1. Burotto, M., Chiou, V. L., Lee, J. M., and Kohn, E. C. (2014) The MAPK pathway across different malignancies: a new perspective. *Cancer* **120**, 3446-3456
2. Flaherty, K. T., Puzanov, I., Kim, K. B., Ribas, A., McArthur, G. A., Sosman, J. A., O'Dwyer, P. J., Lee, R. J., Grippo, J. F., Nolop, K., and Chapman, P. B. (2010) Inhibition of mutated, activated BRAF in metastatic melanoma. *The New England journal of medicine* **363**, 809-819
3. Joseph, E. W., Pratilas, C. A., Poulikakos, P. I., Tadi, M., Wang, W., Taylor, B. S., Halilovic, E., Persaud, Y., Xing, F., Viale, A., Tsai, J., Chapman, P. B., Bollag, G., Solit, D. B., and Rosen, N. (2010) The RAF inhibitor PLX4032 inhibits ERK signaling and tumor cell proliferation in a V600E BRAF-selective manner. *Proceedings of the National Academy of Sciences of the United States of America* **107**, 14903-14908
4. Solit, D. B., Garraway, L. A., Pratilas, C. A., Sawai, A., Getz, G., Basso, A., Ye, Q., Lobo, J. M., She, Y., Osman, I., Golub, T. R., Sebolt-Leopold, J., Sellers, W. R., and Rosen, N. (2006) BRAF mutation predicts sensitivity to MEK inhibition. *Nature* **439**, 358-362
5. Infante, J. R., Fecher, L. A., Falchook, G. S., Nallapareddy, S., Gordon, M. S., Becerra, C., DeMarini, D. J., Cox, D. S., Xu, Y., Morris, S. R., Peddareddigari, V. G., Le, N. T., Hart, L., Bendell, J. C., Eckhardt, G., Kurzrock, R., Flaherty, K., Burris, H. A., 3rd, and Messersmith, W. A. (2012) Safety, pharmacokinetic, pharmacodynamic, and efficacy data for the oral MEK inhibitor trametinib: a phase 1 dose-escalation trial. *The Lancet. Oncology* **13**, 773-781
6. Flaherty, K. T., Robert, C., Hersey, P., Nathan, P., Garbe, C., Milhem, M., Demidov, L. V., Hassel, J. C., Rutkowski, P., Mohr, P., Dummer, R., Trefzer, U., Larkin, J. M., Utikal, J., Dreno, B., Nyakas, M., Middleton, M. R., Becker, J. C., Casey, M., Sherman, L. J., Wu, F. S., Ouellet, D., Martin, A. M., Patel, K., Schadendorf, D., and Group, M. S. (2012) Improved survival with MEK inhibition in BRAF-mutated melanoma. *The New England journal of medicine* **367**, 107-114
7. Larkin, J., Ascierto, P. A., Dreno, B., Atkinson, V., Liskay, G., Maio, M., Mandala, M., Demidov, L., Stroyakovskiy, D., Thomas, L., de la Cruz-Merino, L., Dutriaux, C., Garbe, C., Sovak, M. A., Chang, I., Choong, N., Hack, S. P., McArthur, G. A., and Ribas, A. (2014) Combined vemurafenib and cobimetinib in BRAF-mutated melanoma. *The New England journal of medicine* **371**, 1867-1876
8. Long, G. V., Stroyakovskiy, D., Gogas, H., Levchenko, E., de Braud, F., Larkin, J., Garbe, C., Jouary, T., Hauschild, A., Grob, J. J., Chiarion Sileni, V., Lebbe, C., Mandala, M., Millward, M., Arance, A., Bondarenko, I., Haanen, J. B., Hansson, J., Utikal, J., Ferraresi, V., Kovalenko, N., Mohr, P., Probachai, V., Schadendorf, D., Nathan, P., Robert, C., Ribas, A., DeMarini, D. J., Irani, J. G., Casey, M., Ouellet, D., Martin, A. M., Le, N., Patel, K., and Flaherty, K. (2014)

- Combined BRAF and MEK inhibition versus BRAF inhibition alone in melanoma. *The New England journal of medicine* **371**, 1877-1888
9. Karoulia, Z., Wu, Y., Ahmed, T. A., Xin, Q., Bollard, J., Krepler, C., Wu, X., Zhang, C., Bollag, G., Herlyn, M., Fagin, J. A., Lujambio, A., Gavathiotis, E., and Poulikakos, P. I. (2016) An Integrated Model of RAF Inhibitor Action Predicts Inhibitor Activity against Oncogenic BRAF Signaling. *Cancer cell* **30**, 485-498
 10. Lito, P., Pratilas, C. A., Joseph, E. W., Tadi, M., Halilovic, E., Zubrowski, M., Huang, A., Wong, W. L., Callahan, M. K., Merghoub, T., Wolchok, J. D., de Stanchina, E., Chandarlapaty, S., Poulikakos, P. I., Fagin, J. A., and Rosen, N. (2012) Relief of profound feedback inhibition of mitogenic signaling by RAF inhibitors attenuates their activity in BRAFV600E melanomas. *Cancer cell* **22**, 668-682
 11. Poulikakos, P. I., Persaud, Y., Janakiraman, M., Kong, X., Ng, C., Moriceau, G., Shi, H., Atefi, M., Titz, B., Gabay, M. T., Salton, M., Dahlman, K. B., Tadi, M., Wargo, J. A., Flaherty, K. T., Kelley, M. C., Misteli, T., Chapman, P. B., Sosman, J. A., Graeber, T. G., Ribas, A., Lo, R. S., Rosen, N., and Solit, D. B. (2011) RAF inhibitor resistance is mediated by dimerization of aberrantly spliced BRAF(V600E). *Nature* **480**, 387-390
 12. Abildgaard, C., and Guldberg, P. (2015) Molecular drivers of cellular metabolic reprogramming in melanoma. *Trends in molecular medicine* **21**, 164-171
 13. Serasinghe, M. N., Wieder, S. Y., Renault, T. T., Elkholi, R., Asciolla, J. J., Yao, J. L., Jabado, O., Hoehn, K., Kageyama, Y., Sesaki, H., and Chipuk, J. E. (2015) Mitochondrial division is requisite to RAS-induced transformation and targeted by oncogenic MAPK pathway inhibitors. *Molecular cell* **57**, 521-536
 14. Wakabayashi, J., Zhang, Z., Wakabayashi, N., Tamura, Y., Fukaya, M., Kensler, T. W., Iijima, M., and Sesaki, H. (2009) The dynamin-related GTPase Drp1 is required for embryonic and brain development in mice. *The Journal of cell biology* **186**, 805-816
 15. Kashatus, J. A., Nascimento, A., Myers, L. J., Sher, A., Byrne, F. L., Hoehn, K. L., Counter, C. M., and Kashatus, D. F. (2015) Erk2 phosphorylation of Drp1 promotes mitochondrial fission and MAPK-driven tumor growth. *Molecular cell* **57**, 537-551
 16. Haq, R., Shoag, J., Andreu-Perez, P., Yokoyama, S., Edelman, H., Rowe, G. C., Frederick, D. T., Hurley, A. D., Nellore, A., Kung, A. L., Wargo, J. A., Song, J. S., Fisher, D. E., Arany, Z., and Widlund, H. R. (2013) Oncogenic BRAF regulates oxidative metabolism via PGC1alpha and MITF. *Cancer cell* **23**, 302-315
 17. Trotta, A. P., and Chipuk, J. E. (2017) Mitochondrial dynamics as regulators of cancer biology. *Cellular and molecular life sciences : CMLS*
 18. Wieder, S. Y., Serasinghe, M. N., Sung, J. C., Choi, D. C., Birge, M. B., Yao, J. L., Bernstein, E., Celebi, J. T., and Chipuk, J. E. (2015) Activation of the Mitochondrial Fragmentation Protein DRP1 Correlates with BRAF(V600E) Melanoma. *The Journal of investigative dermatology* **135**, 2544-2547
 19. Fried, L. E., and Arbiser, J. L. (2009) Honokiol, a multifunctional antiangiogenic and antitumor agent. *Antioxidants & redox signaling* **11**, 1139-1148
 20. Prasad, R., and Katiyar, S. K. (2016) Honokiol, an Active Compound of Magnolia Plant, Inhibits Growth, and Progression of Cancers of Different Organs. *Advances in experimental medicine and biology* **928**, 245-265
 21. Xie, L., Jiang, F., Zhang, X., Alitongbieke, G., Shi, X., Meng, M., Xu, Y., Ren, A., Wang, J., Cai, L., Zhou, Y., Xu, Y., Su, Y., Liu, J., Zeng, Z., Wang, G., Zhou, H., Chen, Q. C., and Zhang, X. K. (2016) Honokiol sensitizes breast cancer cells to TNF-alpha induction of apoptosis by inhibiting Nur77 expression. *British journal of pharmacology* **173**, 344-356
 22. Zhou, B., Li, H., Xing, C., Ye, H., Feng, J., Wu, J., Lu, Z., Fang, J., and Gao, S. (2017) Honokiol induces proteasomal degradation of AML1-ETO oncoprotein via increasing ubiquitin conjugase UbCH8 expression in leukemia. *Biochemical pharmacology* **128**, 12-25

23. Prasad, R., Kappes, J. C., and Katiyar, S. K. (2016) Inhibition of NADPH oxidase 1 activity and blocking the binding of cytosolic and membrane-bound proteins by honokiol inhibit migratory potential of melanoma cells. *Oncotarget* **7**, 7899-7912
24. Pan, J., Zhang, Q., Liu, Q., Komaz, S. M., Kalyanaraman, B., Lubet, R. A., Wang, Y., and You, M. (2014) Honokiol inhibits lung tumorigenesis through inhibition of mitochondrial function. *Cancer prevention research* **7**, 1149-1159
25. Pillai, V. B., Samant, S., Sundaresan, N. R., Raghuraman, H., Kim, G., Bonner, M. Y., Arbiser, J. L., Walker, D. I., Jones, D. P., Gius, D., and Gupta, M. P. (2015) Honokiol blocks and reverses cardiac hypertrophy in mice by activating mitochondrial Sirt3. *Nature communications* **6**, 6656
26. Salabei, J. K., Gibb, A. A., and Hill, B. G. (2014) Comprehensive measurement of respiratory activity in permeabilized cells using extracellular flux analysis. *Nature protocols* **9**, 421-438
27. Renault, T. T., Floros, K. V., and Chipuk, J. E. (2013) BAK/BAX activation and cytochrome c release assays using isolated mitochondria. *Methods* **61**, 146-155
28. Wittig, I., Carrozzo, R., Santorelli, F. M., and Schagger, H. (2006) Supercomplexes and subcomplexes of mitochondrial oxidative phosphorylation. *Biochimica et biophysica acta* **1757**, 1066-1072
29. Dudkina, N. V., Eubel, H., Keegstra, W., Boekema, E. J., and Braun, H. P. (2005) Structure of a mitochondrial supercomplex formed by respiratory-chain complexes I and III. *Proceedings of the National Academy of Sciences of the United States of America* **102**, 3225-3229
30. Otera, H., Ishihara, N., and Mihara, K. (2013) New insights into the function and regulation of mitochondrial fission. *Biochimica et biophysica acta* **1833**, 1256-1268
31. Viollet, B., Guigas, B., Sanz Garcia, N., Leclerc, J., Foretz, M., and Andreelli, F. (2012) Cellular and molecular mechanisms of metformin: an overview. *Clinical science* **122**, 253-270
32. Lin, C. J., Chen, T. L., Tseng, Y. Y., Wu, G. J., Hsieh, M. H., Lin, Y. W., and Chen, R. M. (2016) Honokiol induces autophagic cell death in malignant glioma through reactive oxygen species-mediated regulation of the p53/PI3K/Akt/mTOR signaling pathway. *Toxicology and applied pharmacology* **304**, 59-69
33. Zhang, Y., Ren, X., Shi, M., Jiang, Z., Wang, H., Su, Q., Liu, Q., Li, G., and Jiang, G. (2014) Downregulation of STAT3 and activation of MAPK are involved in the induction of apoptosis by HNK in glioblastoma cell line U87. *Oncology reports* **32**, 2038-2046
34. Kashatus, D. F., Lim, K. H., Brady, D. C., Pershing, N. L., Cox, A. D., and Counter, C. M. (2011) RALA and RALBP1 regulate mitochondrial fission at mitosis. *Nature cell biology* **13**, 1108-1115
35. Taguchi, N., Ishihara, N., Jofuku, A., Oka, T., and Mihara, K. (2007) Mitotic phosphorylation of dynamin-related GTPase Drp1 participates in mitochondrial fission. *The Journal of biological chemistry* **282**, 11521-11529
36. Kwon, Y. G., Lee, S. Y., Choi, Y., Greengard, P., and Nairn, A. C. (1997) Cell cycle-dependent phosphorylation of mammalian protein phosphatase 1 by cdc2 kinase. *Proceedings of the National Academy of Sciences of the United States of America* **94**, 2168-2173
37. Arora, S., Bhardwaj, A., Srivastava, S. K., Singh, S., McClellan, S., Wang, B., and Singh, A. P. (2011) Honokiol arrests cell cycle, induces apoptosis, and potentiates the cytotoxic effect of gemcitabine in human pancreatic cancer cells. *PloS one* **6**, e21573
38. Deng, J., Qian, Y., Geng, L., Chen, J., Wang, X., Xie, H., Yan, S., Jiang, G., Zhou, L., and Zheng, S. (2008) Involvement of p38 mitogen-activated protein kinase pathway in honokiol-induced apoptosis in a human hepatoma cell line (hepG2). *Liver international : official journal of the International Association for the Study of the Liver* **28**, 1458-1464
39. Baudy, A. R., Dogan, T., Flores-Mercado, J. E., Hoefflich, K. P., Su, F., van Bruggen, N., and Williams, S. P. (2012) FDG-PET is a good biomarker of both early response and acquired resistance in BRAFV600 mutant melanomas treated with vemurafenib and the MEK inhibitor GDC-0973. *EJNMMI research* **2**, 22
40. McArthur, G. A., Puzanov, I., Amaravadi, R., Ribas, A., Chapman, P., Kim, K. B., Sosman, J. A., Lee, R. J., Nolop, K., Flaherty, K. T., Callahan, J., and Hicks, R. J. (2012) Marked,

- homogeneous, and early [18F]fluorodeoxyglucose-positron emission tomography responses to vemurafenib in BRAF-mutant advanced melanoma. *Journal of clinical oncology : official journal of the American Society of Clinical Oncology* **30**, 1628-1634
41. Cancer Genome Atlas, N. (2015) Genomic Classification of Cutaneous Melanoma. *Cell* **161**, 1681-1696
 42. Haarberg, H. E., and Smalley, K. S. (2014) Resistance to Raf inhibition in cancer. *Drug discovery today. Technologies* **11**, 27-32
 43. Zhang, G., Frederick, D. T., Wu, L., Wei, Z., Krepler, C., Srinivasan, S., Chae, Y. C., Xu, X., Choi, H., Dimwamwa, E., Ope, O., Shannan, B., Basu, D., Zhang, D., Guha, M., Xiao, M., Randell, S., Sproesser, K., Xu, W., Liu, J., Karakousis, G. C., Schuchter, L. M., Gangadhar, T. C., Amaravadi, R. K., Gu, M., Xu, C., Ghosh, A., Xu, W., Tian, T., Zhang, J., Zha, S., Liu, Q., Brafford, P., Weeraratna, A., Davies, M. A., Wargo, J. A., Avadhani, N. G., Lu, Y., Mills, G. B., Altieri, D. C., Flaherty, K. T., and Herlyn, M. (2016) Targeting mitochondrial biogenesis to overcome drug resistance to MAPK inhibitors. *The Journal of clinical investigation* **126**, 1834-1856
 44. Cogliati, S., Frezza, C., Soriano, M. E., Varanita, T., Quintana-Cabrera, R., Corrado, M., Cipolat, S., Costa, V., Casarin, A., Gomes, L. C., Perales-Clemente, E., Salviati, L., Fernandez-Silva, P., Enriquez, J. A., and Scorrano, L. (2013) Mitochondrial cristae shape determines respiratory chain supercomplexes assembly and respiratory efficiency. *Cell* **155**, 160-171
 45. Kasznicki, J., Sliwinska, A., and Drzewoski, J. (2014) Metformin in cancer prevention and therapy. *Annals of translational medicine* **2**, 57
 46. Weinberg, S. E., and Chandel, N. S. (2015) Targeting mitochondria metabolism for cancer therapy. *Nature chemical biology* **11**, 9-15
 47. Liu, Z., Zhang, X., Cui, W., Zhang, X., Li, N., Chen, J., Wong, A. W., and Roberts, A. (2007) Evaluation of short-term and subchronic toxicity of magnolia bark extract in rats. *Regulatory toxicology and pharmacology : RTP* **49**, 160-171
 48. Zhang, Q., Li, J., Zhang, W., An, Q., Wen, J., Wang, A., Jin, H., and Chen, S. (2015) Acute and sub-chronic toxicity studies of honokiol microemulsion. *Regulatory toxicology and pharmacology : RTP* **71**, 428-436
 49. Cerella, C., Radogna, F., Dicato, M., and Diederich, M. (2013) Natural compounds as regulators of the cancer cell metabolism. *International journal of cell biology* **2013**, 639401
 50. Chen, T., Li, J., Liu, J., Li, N., Wang, S., Liu, H., Zeng, M., Zhang, Y., and Bu, P. (2015) Activation of SIRT3 by resveratrol ameliorates cardiac fibrosis and improves cardiac function via the TGF-beta/Smad3 pathway. *American journal of physiology. Heart and circulatory physiology* **308**, H424-434
 51. Singh, T., Gupta, N. A., Xu, S., Prasad, R., Velu, S. E., and Katiyar, S. K. (2015) Honokiol inhibits the growth of head and neck squamous cell carcinoma by targeting epidermal growth factor receptor. *Oncotarget* **6**, 21268-21282
 52. Vaid, M., Sharma, S. D., and Katiyar, S. K. (2010) Honokiol, a phytochemical from the Magnolia plant, inhibits photocarcinogenesis by targeting UVB-induced inflammatory mediators and cell cycle regulators: development of topical formulation. *Carcinogenesis* **31**, 2004-2011
 53. Hahm, E. R., and Singh, S. V. (2007) Honokiol causes G0-G1 phase cell cycle arrest in human prostate cancer cells in association with suppression of retinoblastoma protein level/phosphorylation and inhibition of E2F1 transcriptional activity. *Molecular cancer therapeutics* **6**, 2686-2695
 54. Asghar, U., Witkiewicz, A. K., Turner, N. C., and Knudsen, E. S. (2015) The history and future of targeting cyclin-dependent kinases in cancer therapy. *Nature reviews. Drug discovery* **14**, 130-146
 55. Gelles, J. D., and Chipuk, J. E. (2016) Robust high-throughput kinetic analysis of apoptosis with real-time high-content live-cell imaging. *Cell death & disease* **7**, e2493

FOOTNOTES

This work was supported by: NIH grants CA157740 (J.E.C.), CA206005 (J.E.C.), and AR4790 (J.L.A); the JJR Foundation, the William A. Spivak Fund, the Fridolin Charitable Trust, the Rabinowitch-Davis Foundation, an American Cancer Society Research Scholar Award, a Leukemia & Lymphoma Society Career Development Award, and an Irma T. Hirschl/Monique Weill-Caulier Trust Research Award. This work was also supported in part by two research grants (5FY1174 and 1FY13416) from the March of Dimes Foundation, the Developmental Research Pilot Project Program within the Department of Oncological Sciences at the Icahn School of Medicine at Mount Sinai and the Tisch Center Institute - Cancer Center Support Grant P30 CA196521.

The abbreviations used are: Honokiol, HKL; electron transport chain, ETC; oxygen consumption rate, OCR; dynamin-related protein 1, DRP1; reactive oxygen species, ROS; NADH dehydrogenase, ND; cyclin dependent kinase, CDK.

A375	%G1±SEM	%S±SEM	%G2/M±SEM
DMSO	57±0.27	28±1.1	15±0.48
40µM HKL	63±1.8	27±2.2	11±0.68
1µM PLX	92±0.13	2±2.9	6±0.42

SKMEL-28	%G1±SEM	%S±SEM	%G2/M±SEM
DMSO	65±0.53	27±0.64	8±0.88
40µM HKL	88±2.2	10±3	2.2±0.89
1µM PLX	93±0.78	5±0.09	2±0.70

MeWo	%G1±SEM	%S±SEM	%G2/M±SEM
DMSO	54±1.3	37±1.1	9.1±0.39
40µM HKL	69±0.28	14±3.7	17±3.9
1µM PLX	50±0.41	41±0.35	10±0.17

Table 1: Effect of HKL and PLX-4032 on cell cycle profiles. Data represent mean percentage of cells in each cell cycle phase ± SEM.

Figure 1

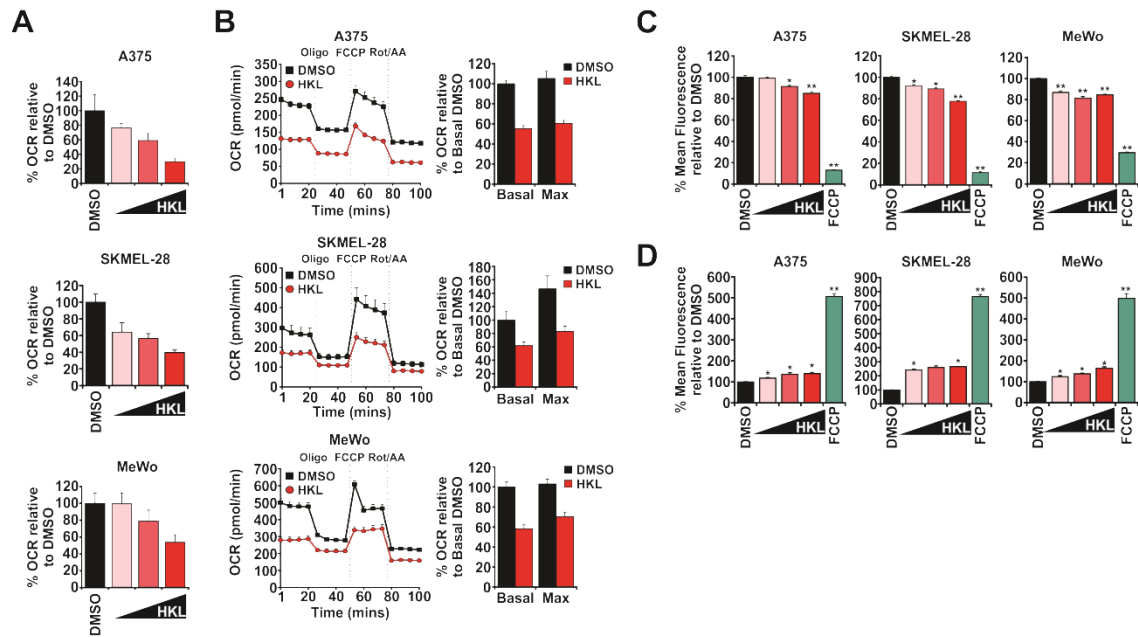


Figure 2

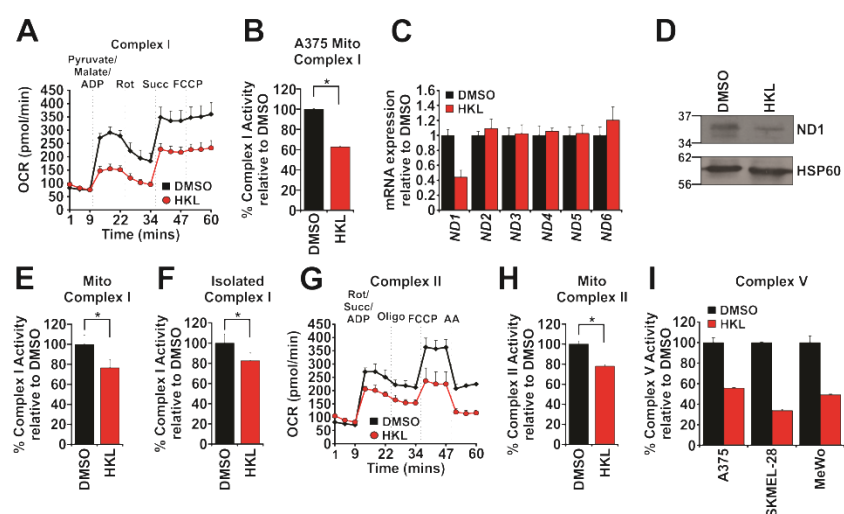


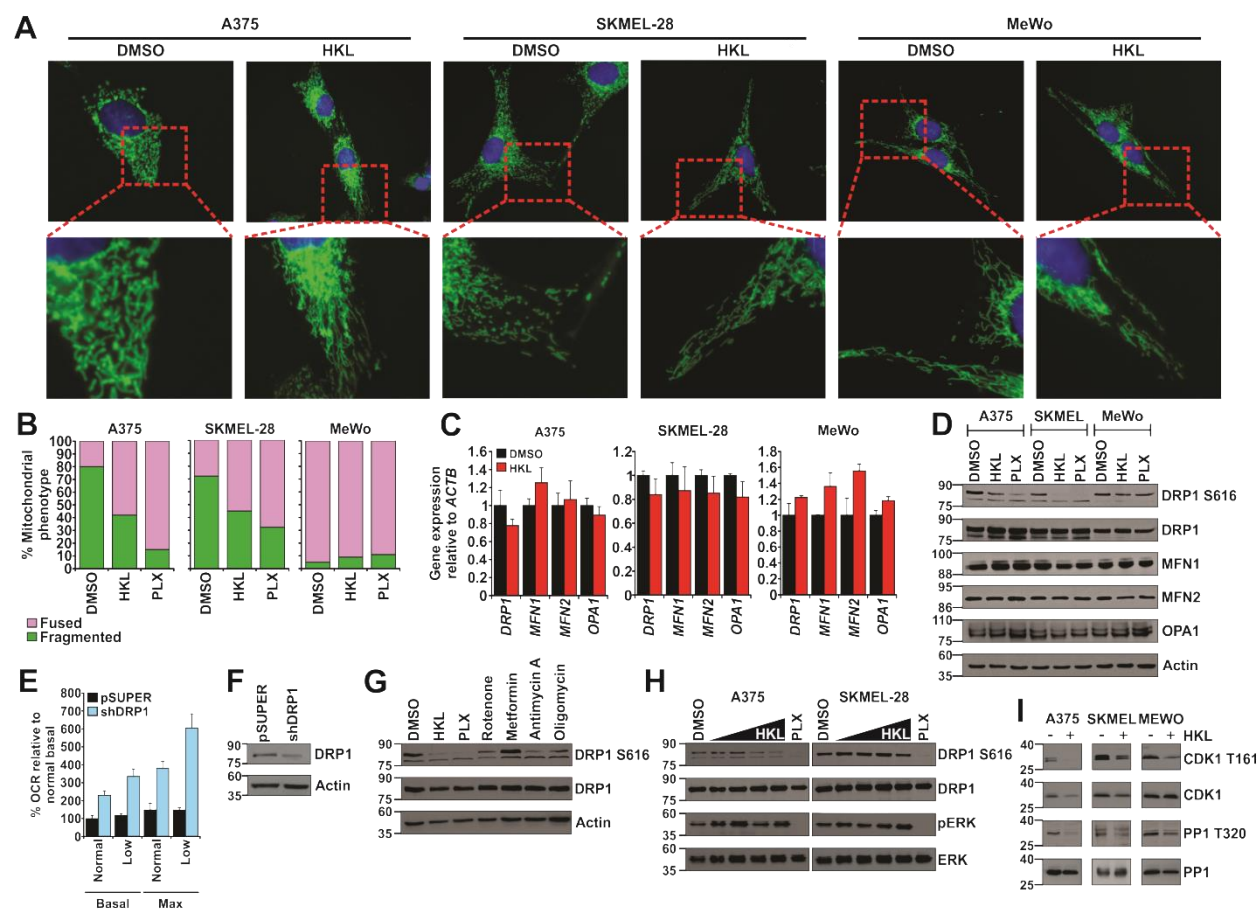
Figure 3

Figure 4

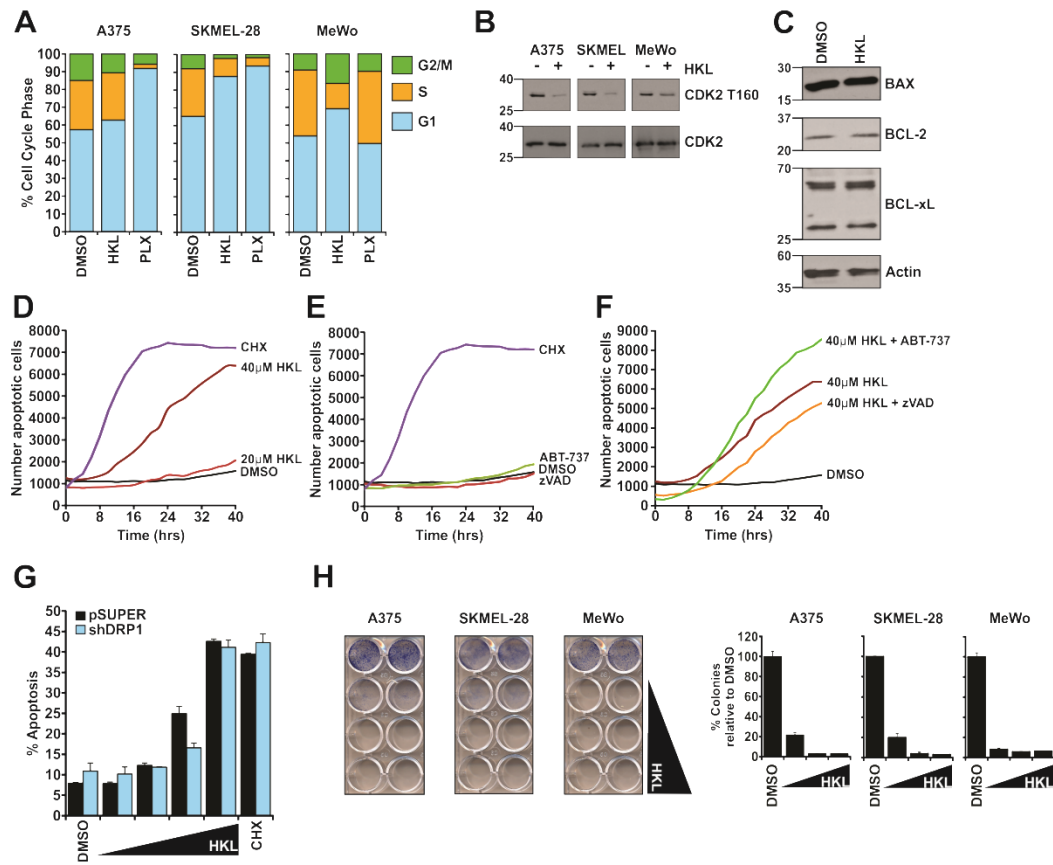


Figure 5

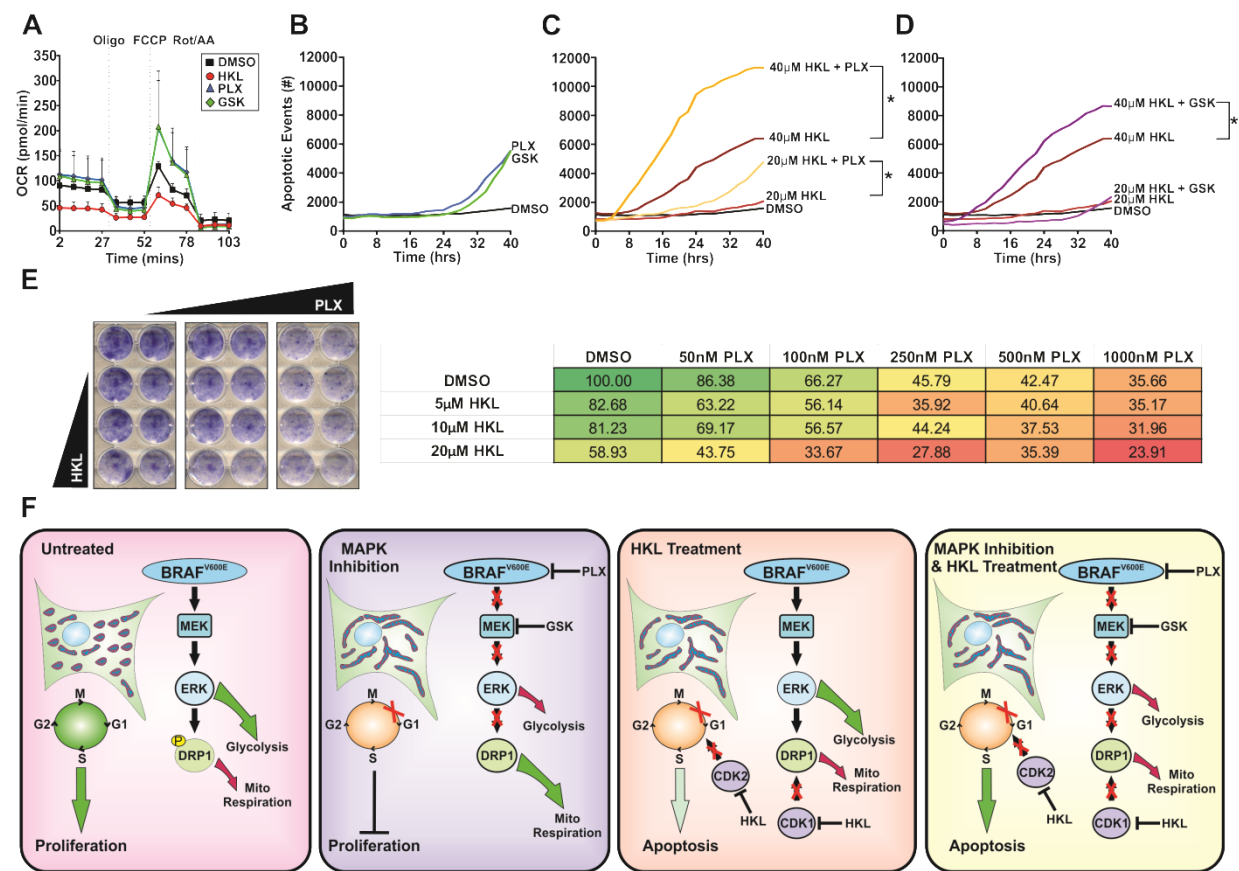


FIGURE LEGENDS

FIGURE 1: HKL promotes mitochondrial dysfunction by inhibiting cellular respiration. (A) Oxygen consumption rates (OCR) were measured in A375, SKMEL-28, and MeWo melanoma cells using a Seahorse Bioanalyzer. DMSO or increasing doses (10, 20, or 40 μ M) HKL were directly administered to cells, incubated for approximately 5 mins, followed by recording of OCR measurements. (B) Melanoma cells were treated with DMSO or HKL (40 μ M) for 8 hrs prior to measuring OCR. Four baseline measurements were taken prior to sequential administration of oligomycin (1 μ M), FCCP (1 μ M), and a combination of rotenone and antimycin A (0.5 μ M). Bar graphs represent the effect HKL has on basal and maximal OCR. (C-D) Melanoma cells were treated with DMSO, increasing doses (10, 20, or 40 μ M) HKL for 8 hrs or FCCP (50 μ M) for 2 hrs. Media was changed and cells were loaded with TMRE (100nM) or MitoSox for 30 mins and analyzed by flow cytometry. Significance denoted by * $p < 0.05$, ** $p < 0.01$, by Student T test. All data is representative of at least three independent experiments, and is reported as mean \pm SEM.

FIGURE 2: HKL-mediated mitochondrial dysfunction occurs through inhibition of electron transport chain complexes I, II, and V. (A) A375 cells were treated with DMSO or HKL (40 μ M) for 8 hrs. Plasma membranes were permeabilized with recombinant perfringolysin O (1nM) for 30 mins at 37°C. Basal OCR were measured in a Seahorse bioanalyzer before sequential administration of a combination of pyruvate (10mM), malate (0.5mM), and ADP (4mM), succinate (10mM), and FCCP (1 μ M). (B) Complex I enzymatic activity was measured from A375 cells treated with DMSO or HKL (40 μ M) for 24 hrs. Mitochondrial fractions were isolated and assessed for complex I activity. (C) Quantitative real time PCR analysis of nicotinamide dehydrogenase (ND) subunits 1-6 from mRNA extracted from A375 cells treated with DMSO or HKL (40 μ M) for 24 hrs. Gene expression was normalized to *ACTB*. (D) Western blot analysis of ND1 protein levels from isolated mitochondrial fractions from A375 cells treated with either DMSO or HKL (40 μ M) for 24 hrs. Hsp60 was used as a loading control. (E) Complex I enzymatic activity was measured from mouse liver mitochondrial extracts treated with DMSO or HKL (40 μ M) for 30 mins at room temperature. (F) Mouse liver mitochondria were lysed in complex I extraction buffer and complex I proteins were immunoprecipitated on ELISA plates in the presence of DMSO or HKL (40 μ M). (G) Same as in (A) except following basal OCR measurements, cells were sequentially treated with a combination of rotenone (1 μ M), succinate (10mM), and ADP (4mM), oligomycin (1 μ M), FCCP (1 μ M), and antimycin A (0.5 μ M). (H) Same as in (E) except Complex II enzymatic activity was analyzed. (I) ATP-linked respiration was determined using a Seahorse bioanalyzer. Melanoma cells treated with DMSO or HKL (40 μ M) for 8 hrs were treated with oligomycin (1 μ M) and OCR measurements were recorded. Significance denoted by * $p < 0.05$, by Student T test. All data is representative of three independent experiments, and is reported as mean \pm SEM.

FIGURE 3: HKL causes mitochondrial fusion by downregulating CDK1-mediated DRP1 phosphorylation at serine 616. (A) Melanoma cells were treated with DMSO or HKL (40 μ M) for 24 hrs. Cells were loaded with MitoTracker Green and Hoechst 33342 (nuclei) and imaged. (B) Quantification of mitochondrial phenotypes in A375, SKMEL-28, and MeWo cells. In each treatment group 200 cells were counted and scored as contain either fused or fragmented mitochondria. (C) Quantitative real time PCR analysis of mitochondrial dynamics genes from melanoma cells treated with DMSO or HKL (40 μ M) for 24 hrs. Gene expression was normalized to *ACTB*. (D) Western blot analysis of mitochondrial dynamics proteins from melanoma cells treated with DMSO, HKL (40 μ M), or PLX-4032 (1 μ M) for 24 hrs. Beta actin was used as a loading control. (E) SKMEL-28 shDRP1 (or pSUPER) cells were analyzed for basal and maximal OCRs in the presence of normal (35mM) or low (5mM) glucose. (F) Western blot analysis of DRP1 protein levels in control pSUPER or shDRP1 SKMEL-28 cells. Beta actin was used as a loading control. (G) A375 cells were treated with DMSO, HKL (40 μ M), or 1 μ M of either PLX-4032, rotenone, metformin, antimycin A, or oligomycin for 24 hrs. Protein lysates were analyzed by western blot for phosphorylated DRP1 (DRP1 S616) and total DRP1. Beta actin was

used as a loading control. **(H)** A375 and SKMEL-28 cells were treated with DMSO, increasing doses (10, 20, 30, or 40 μ M) HKL, or PLX-4032 (1 μ M) for 24 hrs. Protein lysates were analyzed by western blot for pDRP1 S616, total DRP1, phosphorylated ERK (pERK), and total ERK. **(I)** Melanoma cells were treated with DMSO or HKL (40 μ M) for 24 hrs. Protein lysates were analyzed by western blot for phosphorylated CDK1 (CDK1 T161), total CDK1, phosphorylated PP1 (PP1 T320) and total PP1. All data is representative of at least three independent experiments, and is reported as mean \pm SEM.

FIGURE 4: HKL induces G1-cell cycle arrest and the mitochondrial pathway of apoptosis. **(A)** Melanoma cells were treated with DMSO, HKL (40 μ M), or PLX-4032 (1 μ M) for 24 hrs and analyzed for cell cycle distribution by flow cytometry. **(B)** Melanoma cells treated the same as in (A) were analyzed by western blot for phosphorylated CDK2 (CDK2 T160) and total CDK2 protein levels. **(C)** A375 cells were treated with DMSO or HKL (40 μ M) for 24 hrs. Protein lysates were analyzed by western blot for components of the apoptotic machinery. Beta actin was used as a loading control. **(D-F)** Kinetic apoptosis assays were performed using an IncuCyte Zoom. A375 cells were treated with DMSO, HKL (20 or 40 μ M), CHX (25 μ g/ml), or ABT-737 (0.5 μ M). Where indicated, cells were treated with zVAD-fmk (50 μ M) for 2 hrs before treatment with HKL. Data represents the number of Annexin V-positive events captured every 2 hrs over a time course of 40 hrs. **(G)** pSUPER or shDRP1 SKMEL-28 cells were treated with DMSO or increasing doses (20, 30, 40, or 50 μ M) HKL for 24 hrs. Apoptosis was measured by Annexin-V staining by flow cytometry. Cycloheximide (CHX) (25 μ g/ml) was used as a positive control for apoptosis. **(H)** Colony formation assays were performed with melanoma cells plated at a density of 8000 cells/well and treated every 2 days with DMSO or increasing doses (40, 50, and 60 μ M) HKL. Once control cells reached confluency, treatments were removed, and cells stained with methylene blue. Graphs represent the percentage of colonies relative to DMSO. All data represents at least three independent experiments, and is reported as mean \pm SEM.

FIGURE 5: HKL-mediated mitochondrial dysfunction potentiates the apoptotic responses of MAPK inhibition. **(A)** A375 cells treated with DMSO, HKL (40 μ M), PLX-4032 (1 μ M), or GSK-1120212 (10nM) for 24 hrs and then analyzed for changes in OCR using a Seahorse Bioanalyzer. Four basal OCR measurements were made before sequential treatment of oligomycin (1 μ M), FCCP (1 μ M), and a combination of rotenone and antimycin A (0.5 μ M). **(B-D)** Kinetic apoptosis assays were performed in A375 cells treated with DMSO, PLX-4032 (10 μ M), GSK-1120212 (10nM), HKL (20 or 40 μ M), or in combination. Annexin V-positive events were captured using an IncuCyte Zoom every 2 hrs over a period of 40 hrs. Significance denoted by * $p < 0.05$, by Student T test. **(E)** Colony formation assays were performed using A375 cells plated at a density of 8000 cells/well and treated with DMSO, increasing doses of HKL (5, 10, or 20 μ M), PLX-4032 (50, 100, 250, 500, or 1000nM), or in combination every 2 days. Cells were stained with methylene blue. Representative percentages of colonies are presented. All data is representative of three independent experiments, and reported as mean \pm SEM. **(F)** Model summarizing the effects of MAPK inhibitors and HKL on cellular metabolism, mitochondrial shape, cell cycle progression, and cell fate. Inhibition of MAPK signaling causes mitochondrial fusion, increased mitochondrial respiration, cell cycle arrest, and decreased proliferation. HKL inhibits mitochondrial respiration, increases mitochondrial fusion, cell cycle arrest, and apoptosis. Combined HKL and inhibition of MAPK signaling significantly enhances apoptotic responses.

Disruption of mitochondrial electron transport chain function potentiates the pro-apoptotic effects of MAPK inhibition.

Andrew P. Trotta, Jesse D. Gelles, Madhavika N. Serasinghe, Patrick Loi, Jack L. Arbiser and Jerry E. Chipuk

J. Biol. Chem. published online May 25, 2017

Access the most updated version of this article at doi: [10.1074/jbc.M117.786442](https://doi.org/10.1074/jbc.M117.786442)

Alerts:

- [When this article is cited](#)
- [When a correction for this article is posted](#)

[Click here](#) to choose from all of JBC's e-mail alerts

Supplemental material:

<http://www.jbc.org/content/suppl/2017/05/25/M117.786442.DC1>

This article cites 0 references, 0 of which can be accessed free at

<http://www.jbc.org/content/early/2017/05/25/jbc.M117.786442.full.html#ref-list-1>